Unbiased RNA–protein interaction screen by quantitative proteomics

Falk Butter[a], Marion Scheibe[b], Mario Mörl[b], and Matthias Mann[a,1]

[a]Department of Proteomics and Signal Transduction, Max Planck Institute for Biochemistry, Am Klopferspitz 18, 82152 Martinsried, Germany; and [b]Institute for Biochemistry, University of Leipzig, Brüderstrasse 34, 04103 Leipzig, Germany

Edited by Joan A. Steitz, Yale University, New Haven, CT, and approved May 6, 2009 (received for review December 5, 2008)

Mass spectrometry (MS)-based quantitative interaction proteomics has successfully elucidated specific protein–protein, DNA–protein, and small molecule–protein interactions. Here, we developed a gel-free, sensitive, and scalable technology that addresses the important area of RNA–protein interactions. Using aptamer-tagged RNA as bait, we captured RNA-interacting proteins from stable isotope labeling by amino acids in cell culture (SILAC)-labeled mammalian cell extracts and analyzed them by high-resolution, quantitative MS. Binders specific to the RNA sequence were distinguished from background by their isotope ratios between bait and control. We demonstrated the approach by retrieving known and novel interaction partners for the HuR interaction motif, H4 stem loop, "zipcode" sequence, tRNA, and a bioinformatically-predicted RNA fold in DGCR-8/Pasha mRNA. In all experiments we unambiguously identified known interaction partners by a single affinity purification step. The 5′ region of the mRNA of DGCR-8/Pasha, a component of the microprocessor complex, specifically interacts with components of the translational machinery, suggesting that it contains an internal ribosome entry site.

quantitative mass spectrometry | ribonucleoprotein | RNA-binding proteins | HuR | internal ribosome entry site

Ribonucleic acid (RNA) is increasingly recognized for its diversity of cellular functions ranging from its classical roles as structural component in complexes such as the ribosome and its role as the central intermediate in gene expression to recently-discovered, critical roles in gene regulation (1). Analysis of RNA can efficiently be performed by hybridization or sequencing-based methods; however, in the cellular environment RNA is associated with RNA-binding proteins (RBPs) forming functional ribonucleoprotein (RNP) complexes. These proteins are essential to the function of RNPs but have been studied much less.

Mass spectrometry (MS)-based proteomics has become a widespread tool for studying complex mixtures of proteins at high sensitivity (2, 3). High-resolution and high-accuracy technologies have recently been introduced at a large scale (4), and entire proteomes can now be quantified (5). Quantitative proteomics has also emerged as a powerful tool for detecting specific binding of proteins to baits by an unbiased proteome-wide screen using peptides and proteins (reviewed in ref. 6) and DNA (7, 8) as baits. These screens have provided candidates that subsequently proved to be of physiological importance in vivo (7, 9, 10). However, application of this technique to detect RBPs has not been reported to our knowledge.

In one technology of quantitative proteomics, stable isotope labeling of amino acids in cell culture (SILAC), 2 cell populations are metabolically encoded with either $^{13}C_6$ (heavy) amino acids or $^{12}C_6$ (light) amino acids (11, 12). Background proteins occur equally in control and bait eluate, and the SILAC peptide pairs consequently have a 1:1 intensity ratio. Specific binders to the bait have heavy/light ratio significantly different from 1:1. We have previously shown that SILAC interaction screens are an efficient assay for detecting interactions of proteins to modified peptides (13, 14) and DNA (8).

Because previous proteomic studies of the protein components of RNPs were nonquantitative they generally suffered from high rates of binding of unspecific RBPs to the RNA baits. Use of quantitative MS has 2 major advantages for RNA affinity purifications. First, the effect of differential stability of the RNA baits in crude extracts is accounted for by normalization on the total amount of background binders in bait pull-down and control. Second, it can detect specific interactions in the presence of highly-abundant background binders, thus near-physiological buffer conditions for incubation and washing can be used to preserve less stable, but specific, interactions.

Here, we describe an in vitro reconstitution system that combines the use of an RNA aptamer, a prerequisite for future ex vivo studies, and high-resolution quantitative MS to detect interaction partners for RNA motifs of general interest.

Results

Design of S1-Aptamer Baits for Gel-Free Quantitative MS Studies. To immobilize the RNA bait on paramagnetic streptavidin beads, we initially investigated the incorporation of biotin-tagged ribonucleotides by in vitro transcription, addition of biotin-ATP by poly(A) polymerase (15), and 3′-splint assisted ligation of biotin-dATP by Klenow fragment (16). Although these methods resulted in immobilized RNA baits, they were not optimal for our purposes because they introduced several randomly-incorporated binding sites per RNA construct, could not be adapted to the required scale, or were too laborious for scale-up. We then investigated an aptamer tag against streptavidin (17). We fused the aptamer to the 3′ end of the RNA instead of introducing it internally (17, 18), which facilitates probe design because RNA structure should not be affected. Because a single copy of the 45-nt minimal aptamer is sufficient to immobilize the RNA baits on paramagnetic streptavidin beads (Fig. S1), we constructed RNA templates by PCR amplification or primer extension with chemically-synthesized oligonucleotides containing the aptameric tag sequence at the 3′ end. This approach circumvents laborious cloning steps. The aptamer strategy turned out to be superior to the alternatives because it ensured complete labeling of all baits and allowed specific elution with biotin, thereby reducing background binders, which in turn enabled gel-free, single-run MS analysis, accelerating sample throughput (Fig. 1). It also allowed the analysis of $<10^7$ cells, much less than what is commonly used in the field.

Identification of HuR Binding to the 3′ UTR of Histone Deacetylase 2 (HDAC2) mRNA by Unbiased Screen. The untranslated sequences at the 5′ or 3′ ends of mRNA molecules bind specific proteins involved in regulating mRNA translation, stability, or localization. To test the ability of our method to detect known, specific binders to such regulatory sequences, we compared protein binding with a se-

Author contributions: F.B. designed research; F.B. and M.S. performed research; F.B. and M.S. analyzed data; and F.B., M.S., M. Mörl, and M. Mann wrote the paper.

The authors declare no conflict of interest.

This article is a PNAS Direct Submission.

Freely available online through the PNAS open access option.

[1]To whom correspondence should be addressed. E-mail: mmann@biochem.mpg.de.

This article contains supporting information online at www.pnas.org/cgi/content/full/0812099106/DCSupplemental.

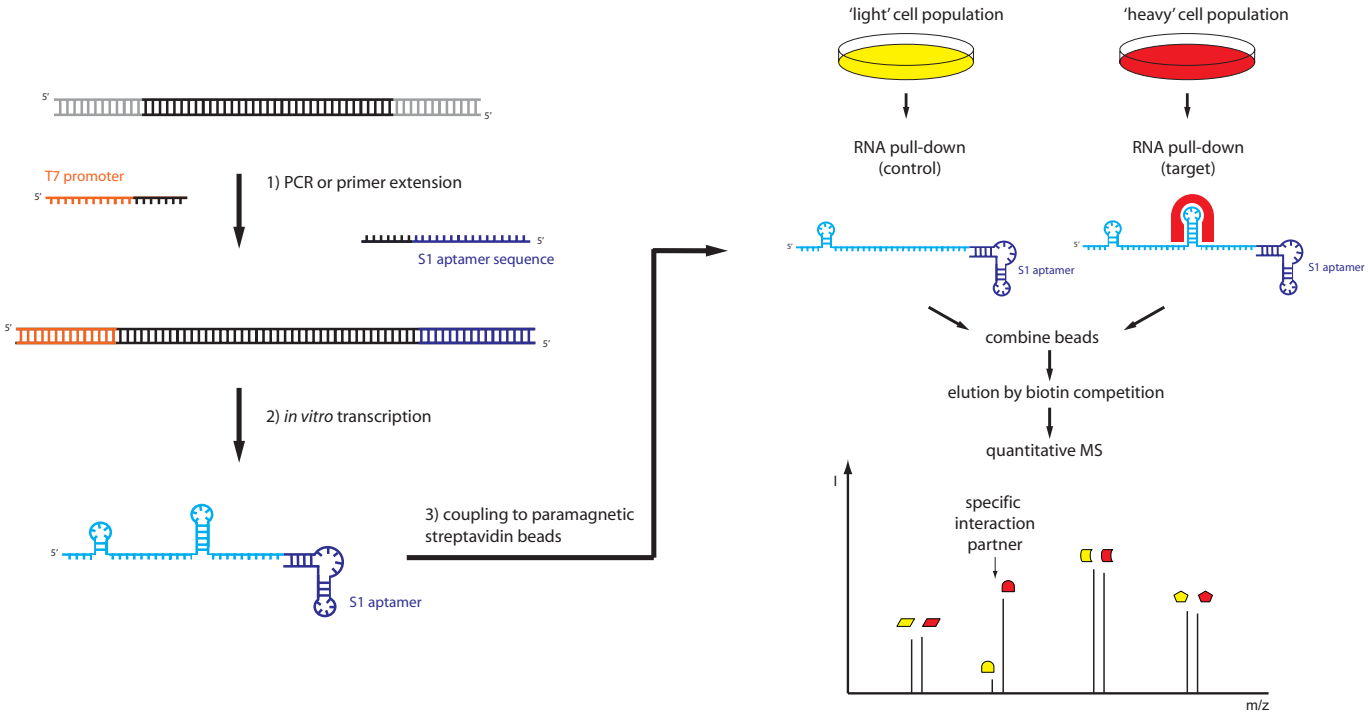

Fig. 1. SILAC-based RNA pull-down. Cells are grown in either media with $^{12}C_6$-Lys/$^{12}C_6$-Arg (light) or $^{13}C_6$-Lys/$^{13}C_6$-Arg (heavy) (11, 12). RNA is immobilized on paramagnetic streptavidin beads by the S1 aptameric tag, which can be introduced by PCR and subsequent in vitro or in vivo transcription. Bait and control sequence are separately incubated with heavy or light cytosolic extracts, respectively. Both fractions are combined after washing, and RNPs are eluted with biotin. Proteins are measured after tryptic digestion and chromatographic separation of the peptides, which are ionized online by electrospray and analyzed with a high-resolution mass spectrometer. The schematic spectrum presents the ratio distribution between light and heavy forms of the tryptic peptides. Specific interaction partners have a SILAC ratio different from the 1:1 ratios of background binders (6).

quence encompassing 292 nt of the 3′ UTR of HDAC2 mRNA harboring an HuR (also known as ELAVL1) hairpin motif already shown to bind HuR (19) with binding to 3 unrelated RNA sequences by using SILAC. For each set of HDAC2 and control RNA we performed 3 pull-downs under 2 different salt conditions (150 and 250 mM NaCl). In these experiments, we included a cross-over pull-down in which the control was incubated with heavy extract, which should lead to inverted ratios for specific binders. Results can then be visualized in 2D plots where proteins fulfilling a specificity threshold in both dimensions are located at the far side of one quadrant (Fig. 2*A*). In all 9 pull-downs we validated HuR as a specific binder to the HDAC2 RNA regulatory sequence (Table S1, Table S2, and Table S3) and reproduced these findings by immunostaining (Fig. 2*B*). Washing with 250 mM salt preserved the known interaction, whereas washing with 150 mM salt led to occasional association of the tRNA synthetase complex. Use of these relatively low concentrations is made possible by the ability of quantitative proteomics to distinguish specific binders by their isotope ratios. We plotted the reverse pull-down (150 mM) against the forward pull-down (250 mM), ensuring that only proteins fulfilling the significance criteria under both conditions were reported (Fig. 2*A*). To retrieve very high confidence interaction partners by our quantitative filtering, we multiplied the outlier probabilities of the forward and reverse screen and implemented a cut-off value of $P < 0.0001$, which can be visualized as a significance area in the plot (gray in the figures). This area automatically adjusts itself to the individual experimental conditions of each pull-down.

To investigate whether our method has detected biological significant interactions occurring in the cell, we performed RNA immunoprecipitation (RIP) on in vivo cross-linked RNPs against HUR and MATR3, one of the significant binders to HDAC2 mRNA. As expected, we detected enrichment of HDAC2 mRNA after HuR immunoprecipitation (19). Furthermore, HDAC2 mRNA was also enriched after MATR3 immunoprecipitation, demonstrating that MATR3 binds to HDAC2 mRNA in vivo (Fig. 2*C*).

Assessing HuR Interactions at Metastasis-Associated Protein 1 (MTA1) Stem Loop Variants. We next tested whether the aptamer strategy is applicable to shorter RNA sequences (≈50 nt), whose structure could possibly be distorted by the tag. We chose a 57-nt sequence of the predicted HuR hairpin located in the 3′ UTR of human MTA1 (19). Again, we detected specific binding of HuR to the wild-type hairpin compared with the hairpin deletion variant (Δ) with a SILAC ratio of 11.8, demonstrating that the tag does not interfere with specific binding to the short hairpin sequence. Next, we compared binding of the hairpin to a control sequence in which we introduced a mutation (AGGA) designed to destabilize the stem loop. As expected, HuR bound to the wild type but not to the destabilized RNA structure as exemplified by a SILAC ratio of 6.5 (Fig. 2*D* and Table S4).

In contrast, when we point-mutated the first position in the stem loop (U15G), we quantified HuR with a 1:1 ratio, indicating that this point mutation is not sufficient to change RNA structure and abrogate binding. This finding is in agreement with evidence that guanine is accepted at this position in the consensus HuR hairpin (19). HuR interaction with the 4 constructs or lack thereof was independently verified by Western blot analysis (Fig. 2*E*). Together, these results demonstrate that the technique is also suited for relatively small RNA probes and that mutation of multiple positions is preferable to point mutations because of the multidimensional folding of RNA structures that may tolerate single-nucleotide exchanges.

Detection of RBPs for H4 mRNA Stem Loop and Zipcode RNA Sequence. To see whether our system is applicable to other RBPs we in vitro-transcribed 2 RNA sequences: the well-studied H4 mRNA

BIOCHEMISTRY

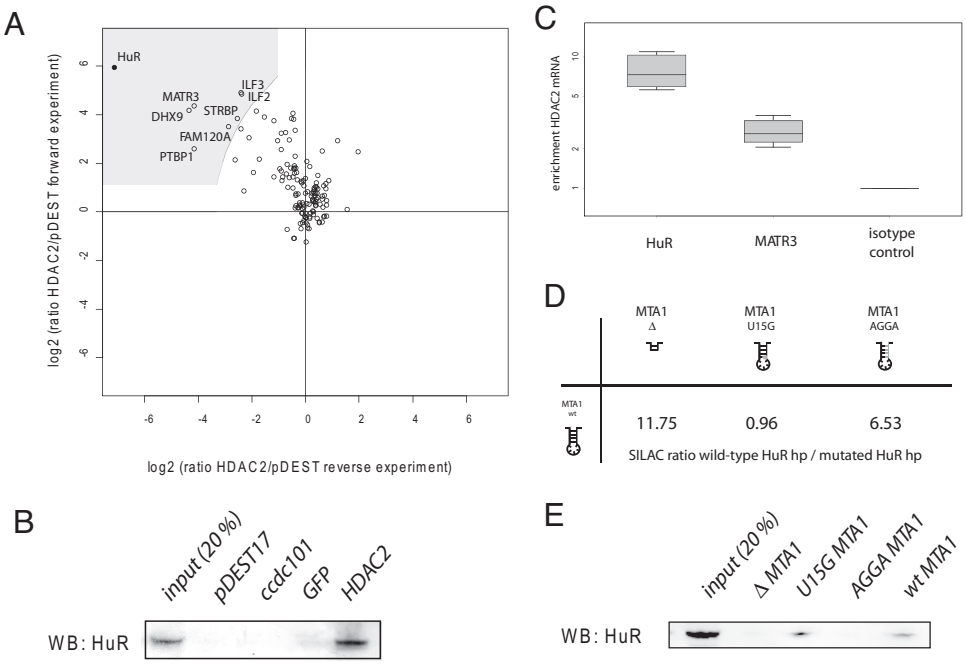

Fig. 2. Detection of HuR. (*A*) 2D plot of RNA pull-down result for HDAC2 mRNA 3′ UTR. The $\log_2$ SILAC ratio of proteins identified with at least 2 unique peptides in each MS run is plotted of the forward pull-down (*x* axis) against the cross-over pull-down (*y* axis). Specific interaction partners show inverse ratios between forward and reverse experiment, grouping them into the upper left quadrant. The interval for statistical significance (shaded in the plot) is given by the product of significance in the forward and reverse experiment ($P^{(for)} \times P^{(rev)} < 0.0001$) and a minimum SILAC ratio change of a factor 2 (expected experimental variation). Among 552 identified proteins before filtering, the known interaction partner for the HDAC2 3′ UTR fragment (HuR) is represented by a black bullet, having the highest SILAC ratio in the forward and smallest in the cross-over experiment. (*B*) Western blot confirmation of the MS analysis for HuR. (*C*) RIP of in vivo cross-linked RNP complexes with antibodies against HUR, MATR3 and isotype control shows enrichment of HDAC2 mRNA at the identified candidates. (*D*) Differential binding of HuR can be detected by comparing MTA1 3′ UTR wild-type sequence with a deletion variant (SILAC ratio 11.8) or a mutated variant with a destabilized stem loop structure (SILAC ratio 6.5). Between the wild-type sequence and a point mutated variant, no differential binding (SILAC ratio 1:1) is observed. (*E*) Results of quantitative MS are supported by Western blot analysis. HuR binds to wild-type sequence and the point mutated variant U15G.

histone stem loop (20) and the β-actin mRNA zipcode (21). As expected, we found the histone stem loop binding protein (SLBP) to interact specifically with the H4 mRNA fragment (Fig. 3*A* and Table S5) and zipcode binding protein 1 (ZBP1) to bind specifically to the zipcode RNA (Fig. 3*B* and Table S6).

For the H4 stem loop, we also detected histone mRNA 3′-exonuclease 1, a known interaction partner (22), with SILAC ratio 6.5 and 0.1 in the cross-over experiments at 150 mM salt. However, because of our stringent selection criteria it is excluded from the plot (see Table S5). Apart from these known interactors, phosphoglycerate mutase family member 5 (PGAM5) interaction is reproducible but has a smaller ratio than SLBP for the histone stem loop.

Zipcode sequences in RNA are thought to localize RNA to specific cellular locations (23). In addition to the known ZBP1 (also known as IMP-1 or IGF2BP1) we found 5 other proteins that bound with significant SILAC ratios: the binding of IMP-3 can readily be rationalized by its close homology to IMP-1 (24) and YB1 has previously been shown to be part of IMP-1 RNP granules (25). Interestingly, CSDA (also known as DBPA) is closely homologous to YB1 (26) and both proteins contain a cold shock domain. IMP-1/IMP-3 and YB1/CSDA are closely related proteins, strongly suggesting biological relevance. Indeed, after our study had been completed, Weidensdorfer et al. (27) identified IMP-3, YB1, and CSDA as in vivo interaction partners by immunoprecipitating

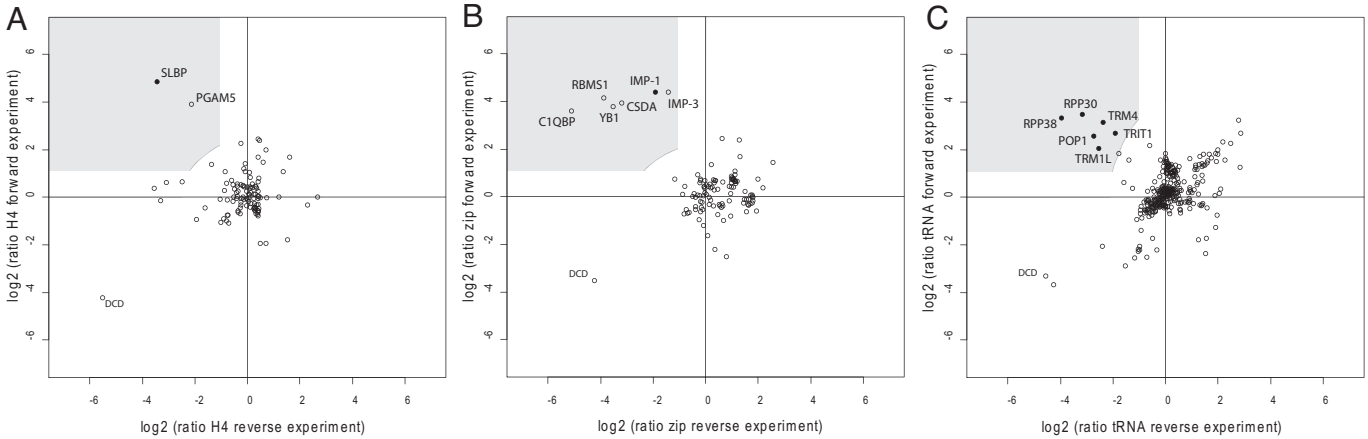

Fig. 3. 2D interaction plots (see Fig. 2) for the identified specific interaction partners for the H4 stem loop, zipcode sequence, and tRNA. (*A*) The H4 stem loop structure specifically interacts with SLBP as indicated by its high SILAC ratio that is inverted in the cross-over experiment. PGAM5 has a smaller SILAC ratio, but binds reproducibly to the H4 stem loop structure compared with the control sequence. Of 641 identified proteins, these are the only 2 proteins fulfilling the stringent quantitation significance criteria. (*B*) Only 6 proteins of 781 identified bound specifically to the zipcode sequence. IMP-1, the known interaction partner, is identified as a specific binder in addition to IMP-3, YB-1, CSDA, RBMS1, and C1QBP. (*C*) RNase P subunits and tRNA enzymatic enzymes are identified as specific binders among 570 identified protein to in vitro-transcribed tRNA. Dermicidine (DCD) is a common contaminant derived from human skin and is therefore unlabeled (very low heavy/light ratio in both pull-downs).

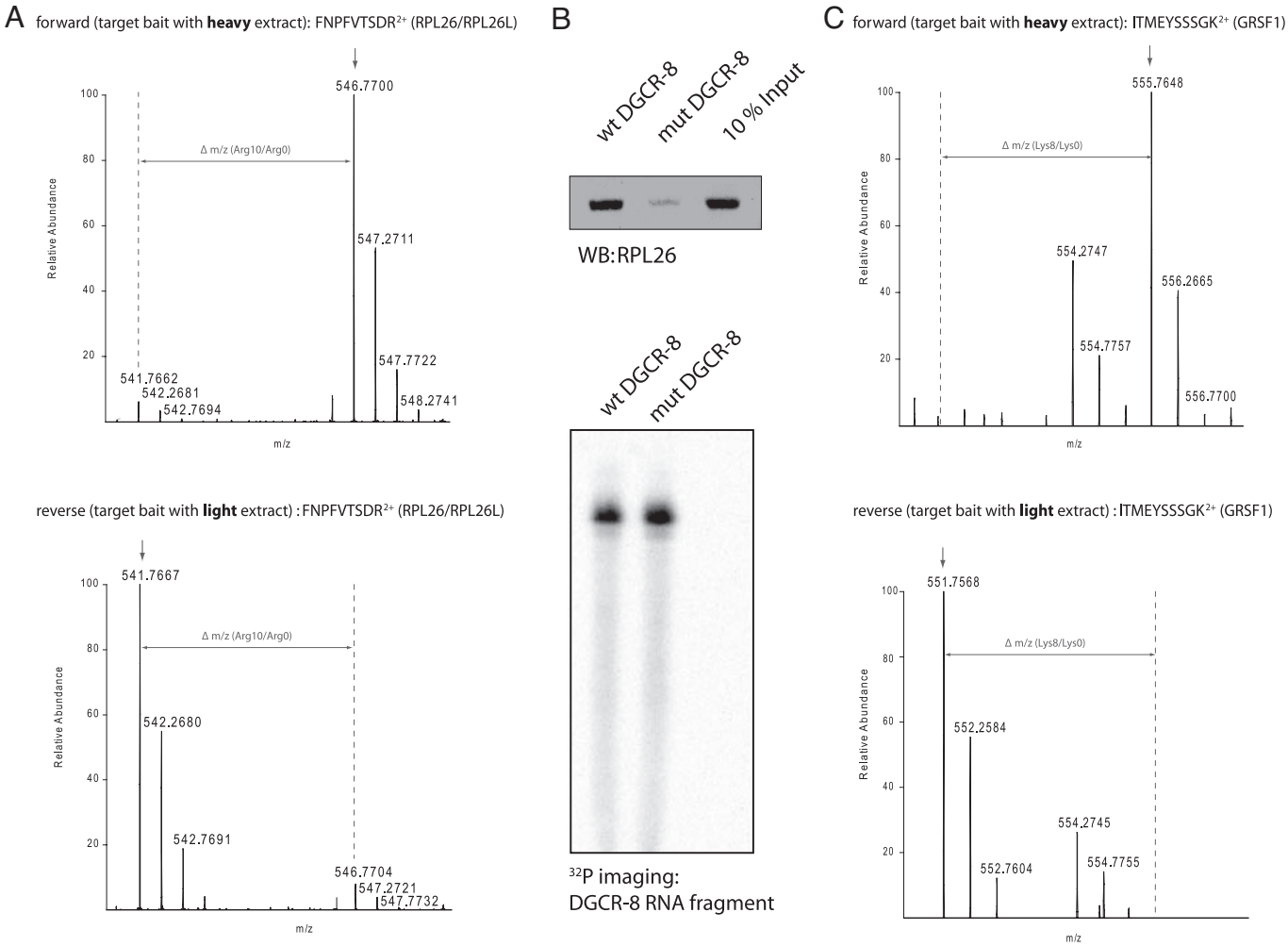

Fig. 4. DGCR-8 RNA pull-down. (*A*) MS identification of RPL26/RPL26L as a specific binder to the DGCR-8 wild-type RNA sequence. The doubly-charged tryptic peptide FNPFVTSDR^{2+} was enriched in the heavy form (heavy extract incubated wild-type sequence) in the forward pull-down, whereas the light form was enriched in the reverse pull-down (light extract incubated with wild-type sequence). (*B*) Immunostaining confirms the binding of RPL26 to the DGCR-8 mRNA fragment observed by quantitative MS. RNA stability in the experiment was monitored by autoradiography of ^{32}P-labeled RNA from the elution fraction. (*C*) The tryptic peptide ITMYSSSGK^{2+} of GRSF1 is also enriched specifically with the wild-type sequence in forward and reverse DGCR-8 RNA pull-down. The corresponding SILAC partner was below the signal to noise, demonstrating that the ratio is >1:10 and 10:1, respectively.

IMP-1. RNA-binding motif single-stranded-interacting protein 1 (RBMS1) and complement component 1 Q subcomponent-binding protein (C1QBP) are statistically significant and highly reproducible interactors to the zipcode sequence, but the biological functions, if any, of these interactions is unclear.

Interactions with Noncoding RNA Molecules. Many RNA molecules in the cell are not messages but are themselves functional end products involved in diverse aspects of cellular activity. To evaluate our method of studying RNA–protein interactions with these types of RNA, we in vitro-transcribed tRNA and aptamer-immobilized it on Dynabeads. We reproducibly detected interactions of enzymes involved in tRNA 5′ processing and tRNA stem loop modification: RNase P subunit p30 (RPP30), RNase P subunit p38 (RPP38), RNase P subunit POP1, tRNA isopentenyltransferase (TRIT1), tRNA N2,N2-dimethylguanosine methyltransferase-like (TRM1L) and tRNA (cytosine-5-)-methyltransferase (TRM4) (Fig. 3*C* and Table S7). tRNA is one of the most heavily-modified RNA molecules, and identification of these tRNA-modifying enzymes suggests that our screen in principle also captures transient interactions. We did not detect 3′-processing enzymes, possibly because of inaccessibility of the tRNA 3′ end caused by the fused aptameric tag. In such cases the tag can be placed at the 5′ end of the sequence.

Identification of a Putative Cellular Internal Ribosome Entry Site (IRES) at a Predicted RNA Fold. Pedersen et al. (28) combined comparative genomic sequencing with RNA folding prediction algorithms, which yielded a large number of interesting and potentially functionally important RNA motifs. We reasoned that our screen could be used to investigate such predicted novel RNA structures with strong evolutionary conservation. We in vitro-transcribed three of the candidate sequences highlighted by Pedersen et al. Two of them did not result in obviously relevant interactors. However, for the stem loop structure in the first exon of the DGCR-8 gene, which is implicated in miRNA processing (29, 30), we reproducibly found specific association of ribosomal protein ($P < 0.05$), which we did not observe with other RNA probes (Table S8). We reconfirmed binding of RPL26, one of the ribosomal proteins detected in our screen (Fig. 4*A*) by immunostaining (Fig. 4*B*). Interestingly, we also found GRSF-1, a protein recruiting mRNAs to polyribosomes (31) and shown to bind to IRESs (32), highly enriched (SILAC ratio 9) at the wild-type sequence (Fig. 4*C*

and Fig. S2). Together, these observations raise the possibility that the conserved structure functions to recruit the ribosome for internal translation.

Discussion

Our method overcomes limitations of current techniques for addressing RNA–protein interactions (33). Unlike bandshift assays with cell extracts, the identity of the RBP can be assessed in a hypothesis-free way. Furthermore, there is no length limitation of the nucleic acid probe as is the case in EMSA or peptide-nucleic acid (PNA)-assisted identification of RBPs (34). Quantitative, high-resolution MS results in high confidence identification of specific RNA–protein interactions from crude cell extracts in a single-step affinity purification at near-physiological conditions. This process is superior to stringent washing conditions followed by band identification, which may lead to identification bias for high-abundant and high-affinity binders. For our method this is exemplified by the detection of specific candidates while the most abundant hnRNPs are quantified by a SILAC ratio of 1:1, identifying them as binders to both the bait and control sequence.

Importantly and unlike in vitro labeling techniques, our strategy enables the quantitative study of in vivo-assembled RNA–protein complexes by transfecting the corresponding plasmid followed by aptamer-based purification from crude cell extracts. This purification procedure has already been demonstrated (17, 18) and will allow future ex vivo studies of RNP complexes by our quantitative proteomic strategy. The approach can be extended to study quantitative, stoichiometric and dynamic changes in protein composition of RNPs in response to stimuli by direct comparison of differentially-labeled cell populations. Indeed, when used for in vivo cross-linked RNP complexes, it represents a complementary approach to RIP (35), which determines RNA components of RNPs.

Here, we used the system to study binding of endogenous HuR from cytoplasmic cell extracts to the predicted MTA1 hairpin structure. We determined common and differential HuR binding to a deletion variant (Δ), a point mutated variant (U15G), and a stem loop-destabilized variant (AGGA), and the wild-type hairpin. The sensitive MS technology used allowed accurate binding studies even when differential binding could barely be detected by immunostaining (Fig. 2*D*). Because our approach does not depend on the availability of antibodies it is applicable to any RNA–protein interaction.

Besides HuR, other proteins were also enriched at the 292-nt-long 3′ UTR fragment of HDAC2. UTRs may contain several RBP interaction motifs (36), and because of the low-salt concentration in our washing steps, secondary protein–protein interactions may be captured, too. As a result, in addition to HuR, we demonstrate the reproducible and statistical significant binding of several other proteins at the HDAC2 mRNA sequence. This group of proteins contains unexpected binders, which would not have been investigated in targeted approaches. We have demonstrated by example that these interactions are likely to also occur in vivo under endogenous protein concentrations; however, their biological roles will need further experimental validation from other techniques.

Interestingly, we found differential binding when comparing proteins associating with coding regions and a 3′-UTR noncoding region (Fig. 2*A*, Table S1, Table S2, and Table S3). Coding regions may not have evolved specific RNA–protein interactions as their sequence is instead dictated by the codon usage for translation, which is further suggested by the fact that no proteins specifically interacted with the control sequence. Thus, our results indicate that it might be feasible to study protein composition of mRNPs by using quantitative MS as a quality filter to detect specific interactions.

Smaller structures of RNA have the advantage of being more well defined and better characterized than long sequences such as UTRs. In those cases we were able to identify already-known interaction partners like SLBP for the H4 histone stem loop, ZBP1 for the zipcode sequence, HuR for the MTA1 hairpin structure, and RNase P for tRNA. These results show that the technique is capable of detecting biologically important RNA–protein interactions. We also identified other candidates with possible biological importance. Most of these interaction partners would not have been identified by a classical hypothesis-driven approach. The clear identification of previously-known biological relevant interactors, the specific binding to the bait compared with the control, and the detection of different specific interaction partners in each experiment strongly suggest nonartifactual interactions. This is also the conclusion from the overall results with the above RNA structures: 6 of 6 tRNA-interacting proteins are in vivo binders, 4 of the 6 binders to the zipcode RNA are already validated as binders in the cell, and for the stem loop structure one of the two found interactors were reported previously to be functional in the cell. Thus, in all cases where independent evidence exists and in all cases in which we performed follow-up experiments the interactions found by quantitative MS also occurred in vivo. Nevertheless, as in any other experimental technique, we cannot rule out that some of our results were caused by limitations of the screen, such as in vitro reconstitution of RNA–protein interaction.

Proteome-wide screening for interaction partners might furthermore be a unique approach to associate predicted RNA folds with a biological function. We have demonstrated that the structure in the DGCR-8 mRNA binds ribosomal proteins and GRSF-1. The hypothesis of a cellular IRES site for this structure awaits further experimental validation, but given the challenges to predict cellular IRES by computational approaches (37) it already constitutes an interesting example for the potential of our screen.

Notably, all steps in our method are scalable. The technique can be performed in single-run MS analysis, making high-throughput studies possible in principle. On-going improvements in sample preparation, processing, and data analysis will allow an increasingly streamlined analysis of RBPs by quantitative MS. Proteome-wide detection of novel RBP candidates for a specific RNA presents a challenge for the study of RNPs, and high-resolution, quantitative MS may bring insights into RNA–protein interactions and RNP composition and function, which are increasingly-important areas of biology.

Materials and Methods

SILAC Cell Extract. HeLa S3 cells were SILAC-labeled in RPMI medium 1640 (−Arg, −Lys) containing 10% dialyzed FBS (Gibco) supplemented with 84 mg/mL $^{13}C_6{}^{15}N_4$ L-arginine and 40 mg/mL $^{13}C_6{}^{15}N_2$ L-lysine (Sigma/Isotec) or the corresponding nonlabeled amino acids, respectively. Three consecutive batches of cells were independently harvested, and cell extracts were prepared as described by Dignam et al. (38) For this study, the cytosolic fraction of this extraction procedure was used.

Production of RNA Templates. To create long (>50 bp) RNA templates forward primers containing the T7 promoter and reverse primers with the S1 aptamer sequence were used in a PCR amplification on a plasmid (*SI Text*). For shorter fragments primer extensions of chemically-synthesized DNA oligos containing either the T7 promoter or the S1 aptamer sequence was performed. In vitro transcription was done according to the manufacturer's protocol (Fermentas), and tagged RNA oligonucleotides were purified with G-50 micro spin columns (GE Healthcare). For radioactive labeling 2.5 μCi [^{32}]ATP was added to the reaction. Successful in vitro transcription was monitored by running an aliquot of the reaction on 10% denaturing PAGE (Rotiphorese), staining with ethidium bromide, and subsequent UV detection. RNA concentration was assessed by A280 absorbance on a Nanodrop (Peqlab).

RNA Pull-Down. S1-tagged RNA (25 μg) was bound to paramagnetic streptavidin C-1 beads (Invitrogen) in RNA binding buffer [100 mM NaCl, 50 mM Hepes·HCl (pH 7.4), 0.5% Nonidet P-40, 10 mM $MgCl_2$] and incubated by shaking for 30 min at 6 °C. Beads were washed 3 times [150 or 250 mM NaCl, 50 mM Hepes·HCl (pH 7.4), 0.5% Nonidet P-40, 10 mM $MgCl_2$], before incubation for 30 min at 6 °C with 400 μg of cytoplasmic extract, 40 units of RNase inhibitor (Fermentas), and 20 μg of yeast tRNA (Invitrogen). After light washing, fractions were combined and RNA was competed from the beads with buffer containing 16 mM biotin. The ethanol-precipitated supernatant was either resuspended in 4× LDS buffer (Invitrogen)

for Western blot analysis or 6 M urea/2 M thiourea (Sigma) for subsequent MS analysis. For Western blot analysis, fractions were run on a Novex 4–12% gradient gel (Invitrogen), transferred to a Protran 85 membrane (Whatman), and probed with 3E2 monoclonal HuR antibody (SCBT) and polyclonal RPL26 antibody (Abcam). A goat-anti-mouse-IgG or donkey-anti-rabbit-IgG phosphatase conjugate (Sigma) together with a BCIP/NBT-Blue liquid substrate system (Sigma) for membranes was used for detection.

For the 3′ binding tests, radioactivity of the fractions was measured with a Bioscan/QC 4000 XER while eluted fractions containing radioactive-labeled RNA were separated by 10% denaturing PAGE and detected by autoradiography on a Storm 860 Optical Scanner (Molecular Dynamics).

MS Data Acquisition and Data Analysis. In-solution digestion and MS analysis was performed essentially as described (39) Peptides were desalted on Stage Tips (40) and analyzed by nanoflow liquid chromatography on an EASY-nLC system from Proxeon Biosystems coupled to a LTQ-Orbitrap XL (Thermo Electron). Peptides were separated on a C18-reversed-phase column packed with Reprosil and directly mounted on the electrospray ion source on an LTQ-Orbitrap XL. We used a 140-min gradient from 2% to 60% acetonitrile in 0.5% acetic acid at a flow of 200 nL/min. The LTQ-Orbitrap XL was operated with a Top5 MS/MS spectra acquisition method in the linear ion trap per MS full scan in the orbitrap. The raw files were processed with MaxQuant (version 1.0.11.5) and searched with the Mascot search engine (Matrix Science) against a IPI human v3.37 protein database concatenated with a decoy of the reversed sequences. Carbamidomethylation was set as fixed modification while methionine oxidation and protein N-acetylation were considered as variable modifications. The search was performed with an initial mass tolerance of 7 ppm mass accuracy for the precursor ion and 0.5 Da for the MS/MS spectra. Search results were processed with MaxQuant (41, 42) filtered with a false discovery rate of 0.01. Before statistical analysis, known contaminants and reverse hits were removed. Only proteins identified with at least 2 unique peptides and 2 quantitation events were considered for analysis. Tables S1–7 contain all proteins identified with $P < 0.05$ in forward or cross-over experiments. The protein ratios of a forward experiment and the corresponding cross-over experiment, together with the interpolated significance curve ($P^{(for)} \times P^{(rev)} < 0.0001$), were plotted in R (prerelease version 2.8.0).

RIP. RIP experiments were basically conducted as described (19). In short, HeLa cells were cross-linked with formaldehyde, quenched by glycine, and sonicated. For each immunoprecipitation protein extract of 2.7×10^7 cells was incubated with 100 μL of antibody-coated Protein A Separose beads (Sigma) for 1.5 h at room temperature. Antibodies for HuR and MATR3 were obtained from Santa Cruz, and murine IGG1 isotype control was from Sigma. After extensive washing with RIPA buffer (containing 0.5 M NaCl) and NT2 buffer the beads were incubated with DNase I buffer containing 40 units of DNase I for 15 min at 30 °C. The beads were washed twice with RIPA buffer, resuspended in 250 μL of elution buffer, and incubated for 45 min at 70 °C to reverse the cross-link. RNA was purified by chloroform-phenol extraction and subsequent ethanol precipitation. cDNA was prepared with a Fermentas cDNA Kit. Quantitative RT-PCR was performed with specific primers for HDAC2 (GGACTATCGCCCCCACGTTT and GGGTCATGCGGATTCTATGAGG) and GAPDH (TGGTATCGTGGAAGGACTCATGAC and ATGCCAGTGAGCTTCCCGTTCAGC) using the iQ SYBR Green Supermix (Bio-Rad). Data were processed by using the modified REST algorithm of the qPCR package (version 1.1–8) for R with standard settings (43).

ACKNOWLEDGMENTS. We thank Johannes Graumann and Jürgen Cox for help with statistical analysis and Michiel Vermeulen (Max Planck Institute for Biochemistry, Martinsried, Germany) for providing extracts. This work was supported by the Max Planck Society and the European Union (Sixth Framework Programs: High-Throughput Epigenetic Regulatory Organisation in Chromatin Grant LSHG-CT). 2005-018883 and Interaction Proteome Grant LSHG-CT-2003-505520.

1. Gesteland RF, Cech T, Atkins JF (2006) *The RNA World: The Nature of Modern RNA Suggests a Prebiotic RNA World* (Cold Spring Harbor Lab Press, Cold Spring Harbor, NY).
2. Aebersold R, Mann M (2003) Mass spectrometry-based proteomics. *Nature* 422:198–207.
3. Cravatt BF, Simon GM, Yates JR, 3rd (2007) The biological impact of mass-spectrometry-based proteomics *Nature* 450:991–1000.
4. Mann M, Kelleher NL (2008) Precision proteomics: The case for high resolution and high mass accuracy. *Proc Natl Acad Sci USA* 105:18132–18138.
5. de Godoy LM, et al. (2008) Comprehensive mass spectrometry-based proteome quantification of haploid versus diploid yeast. *Nature* 455:1251–1254.
6. Vermeulen M, Hubner NC, Mann M (2008) High confidence determination of specific protein–protein interactions using quantitative mass spectrometry. *Curr Opin Biotechnol* 19:331–337.
7. Ranish JA, et al. (2004) Identification of TFB5, a new component of general transcription and DNA repair factor IIH. *Nat Genet* 36:707–713.
8. Mittler G, Butter F, Mann M (2009) A SILAC-based DNA protein interaction screen that identifies candidate binding proteins to functional DNA elements. *Genome Res* 19:284–293.
9. Vermeulen M, et al. (2007) Selective anchoring of TFIID to nucleosomes by trimethylation of histone H3 lysine 4. *Cell* 131:58–69.
10. Christofk HR, Vander Heiden MG, Wu N, Asara JM, Cantley LC (2008) Pyruvate kinase M2 is a phosphotyrosine-binding protein. *Nature* 452:181–186.
11. Ong SE, et al. (2002) Stable isotope labeling by amino acids in cell culture, SILAC, as a simple and accurate approach to expression proteomics. *Mol Cell Proteomics* 1:376–386.
12. Mann M (2006) Functional and quantitative proteomics using SILAC. *Nat Rev Mol Cell Biol* 7:952–958.
13. Hanke S, Mann M (2009) Phosphotyrosine interactome of the insulin receptor family and its substrates IRS-1 and IRS-2. *Mol Cell Proteomics* 8:519–534.
14. Schulze WX, Mann M (2004) A novel proteomic screen for peptide–protein interactions. *J Biol Chem* 279:10756–10764.
15. Martin G, Keller W (1998) Tailing and 3′-end labeling of RNA with yeast poly(A) polymerase and various nucleotides. *RNA* 4:226–230.
16. Huang Z, Szostak JW (1996) A simple method for 3′-labeling of RNA. *Nucleic Acids Res* 24:4360–4361.
17. Srisawat C, Engelke DR (2001) Streptavidin aptamers: Affinity tags for the study of RNAs and ribonucleoproteins. *RNA* 7:632–641.
18. Vasudevan S, Steitz JA (2007) AU-rich-element-mediated up-regulation of translation by FXR1 and Argonaute 2. *Cell* 128:1105–1118.
19. Lopez de Silanes I, Zhan M, Lal A, Yang X, Gorospe M (2004) Identification of a target RNA motif for RNA-binding protein HuR. *Proc Natl Acad Sci USA* 101:2987–2992.
20. Battle DJ, Doudna JA (2001) The stem-loop binding protein forms a highly stable and specific complex with the 3′ stem loop of histone mRNAs. *RNA* 7:123–132.
21. Ross AF, Oleynikov Y, Kislauskis EH, Taneja KL, Singer RH (1997) Characterization of a β-actin mRNA zipcode-binding protein. *Mol Cell Biol* 17:2158–2165.
22. Dominski Z, Yang XC, Kaygun H, Dadlez M, Marzluff WF (2003) A 3′ exonuclease that specifically interacts with the 3′ end of histone mRNA. *Mol Cell* 12:295–305.
23. Kindler S, Wang H, Richter D, Tiedge H (2005) RNA transport and local control of translation. *Annu Rev Cell Dev Biol* 21:223–245.
24. Mori H, et al. (2001) Expression of mouse igf2 mRNA-binding protein 3 and its implications for the developing central nervous system. *J Neurosci Res* 64:132–143.
25. Jonson L, et al. (2007) Molecular composition of IMP1 ribonucleoprotein granules. *Mol Cell Proteomics* 6:798–811.
26. Lu ZH, Books JT, Ley TJ (2006) Cold shock domain family members YB-1 and MSY4 share essential functions during murine embryogenesis. *Mol Cell Biol* 26:8410–8417.
27. Weidensdorfer D, et al. (2009) Control of c-myc mRNA stability by IGF2BP1-associated cytoplasmic RNPs. *RNA* 15:104–115.
28. Pedersen JS, et al. (2006) Identification and classification of conserved RNA secondary structures in the human genome. *PLoS Comput Biol* 2:e33.
29. Denli AM, Tops BB, Plasterk RH, Ketting RF, Hannon GJ (2004) Processing of primary microRNAs by the microprocessor complex. *Nature* 432:231–235.
30. Gregory RI, et al. (2004) The microprocessor complex mediates the genesis of microRNAs. *Nature* 432:235–240.
31. Kash JC, et al. (2002) Selective translation of eukaryotic mRNAs: Functional molecular analysis of GRSF-1, a positive regulator of influenza virus protein synthesis. *J Virol* 76:10417–10426.
32. Cobbold LC, et al. (2008) Identification of internal ribosome entry segment (IRES)-trans-acting factors for the Myc family of IRESs. *Mol Cell Biol* 28:40–49.
33. Lin R-J (2008) *RNA–Protein Interaction Protocols* (Humana, Totowa, NJ).
34. Zielinski J, et al. (2006) In vivo identification of ribonucleoprotein–RNA interactions. *Proc Natl Acad Sci USA* 103:1557–1562.
35. Niranjanakumari S, Lasda E, Brazas R, Garcia-Blanco MA (2002) Reversible cross-linking combined with immunoprecipitation to study RNA–protein interactions in vivo. *Methods* 26:182–190.
36. Hogan DJ, Riordan DP, Gerber AP, Herschlag D, Brown PO (2008) Diverse RNA-binding proteins interact with functionally related sets of RNAs, suggesting an extensive regulatory system. *PLoS Biol* 6:e255.
37. Baird SD, Turcotte M, Korneluk RG, Holcik M (2006) Searching for IRES. *RNA* 12:1755–1785.
38. Dignam JD, Lebovitz RM, Roeder RG (1983) Accurate transcription initiation by RNA polymerase II in a soluble extract from isolated mammalian nuclei. *Nucleic Acids Res* 11:1475–1489.
39. Graumann J, et al. (2008) Stable isotope labeling by amino acids in cell culture (SILAC) and proteome quantitation of mouse embryonic stem cells to a depth of 5,111 proteins. *Mol Cell Proteomics* 7:672–683.
40. Rappsilber J, Ishihama Y, Mann M (2003) Stop and go extraction tips for matrix-assisted laser desorption/ionization, nanoelectrospray, and LC/MS sample pretreatment in proteomics. *Anal Chem* 75:663–670.
41. Cox J, Mann M (2008) MaxQuant enables high peptide identification rates, individualized p.p.b.-range mass accuracies and proteomewide protein quantification. *Nat Biotechnol* 26:1367–1372.
42. Cox J, et al. (2009) A practical guide to the MaxQuant computational platform for SILAC-based quantitative proteomics. *Nat Protoc* 4:698–705.
43. Ritz C, Spiess AN (2008) qpcR: An R package for sigmoidal model selection in quantitative real-time polymerase chain reaction analysis. *Bioinformatics* 24:1549–1551.